Physics of Fluids

RESEARCH ARTICLE | MARCH 05 2021

Examination of laminar Couette flow with obstacles by a low-cost particle image velocimetry setup

Luca Luberto ; Kristin M. de Payrebrune

Physics of Fluids 33, 033603 (2021)
https://doi.org/10.1063/5.0038029

Physics of Fluids ARTICLE scitation.org/journal/phf

Examination of laminar Couette flow with obstacles by a low-cost particle image velocimetry setup

Cite as: Phys. Fluids 33, 033603 (2021); doi: 10.1063/5.0038029
Submitted: 19 November 2020 · Accepted: 12 January 2021 ·
Published Online: 5 March 2021

Luca Luberto[a] and Kristin M. de Payrebrune[b]

AFFILIATIONS

Institute for Computational Physics in Engineering, Technische Universität Kaiserslautern, Erwin-Schrödinger Str., Building 56, 67663 Kaiserslautern, Germany

[a]Author to whom correspondence should be addressed: luca.luberto@mv.uni-kl.de
[b]Electronic mail: kristin.payrebrune@mv.uni-kl.de

ABSTRACT

For many technical applications, a detailed analysis of the fluid mechanical properties is necessary, for which computational fluid dynamics (CFD) simulations are used. However, even though flow simulations are becoming faster and more accurate, validation through experimentation is essential. One way of validation is to use Particle Image Velocimetry (PIV), an imaging technique that can visualize the flow field and measure flow velocities. Since the measuring equipment of commercial systems is very expensive, we propose a low-cost PIV setup that is also affordable for small scientific institutions. In addition to the quality of the acquired images, the reliability and comparability between experiment and simulation are also important issues. Therefore, in this work, we compare the image acquisition quality of the proposed low-cost PIV system with two- and three-dimensional CFD simulations for a laminar Couette flow and a laminar flow around square and hexagonal obstacles with very good agreement. In addition, we analyzed the transferability of 2D and 3D CFD simulations with experiments by measuring the velocity field and found that experimentally determined flow velocities often cannot be used to validate idealized (2D) simulations due to the spatial flow that occurs. However, if the non-ideal conditions of the experiment are considered in the (3D) simulation, a good comparability is given and an experimental validation is possible, for which the presented low-cost PIV system is well suitable.

I. INTRODUCTION

In many areas of industry and research, simulations are used in order to better understand complex processes, to optimize existing systems, and to reduce expensive or time-consuming experiments. However, until a simulation can replace experimental analyses and be used for more advanced questions, the individual steps of the simulation must be checked and compared with reliable data. In flow problems, various visualization methods are used to obtain experimental data of the flow field for comparison with simulations, such as the injection of additional substances (paint/air bubbles/vapor/particles) and application of paint or thin threads to the surface of an overflowed object. If additional velocity or pressure information is needed, Laser Doppler Velocimetry (LDV), hot-wire anemometry, pressure transducers, or Laser to Focus (L2F) method can be used for point measurements and Particle Image Velocimetry (PIV), Magnetic Resonance Velocimetry (MRV), or Doppler Global Velocimetry (DGV) can be used to obtain two-dimensional or spatial vector fields, to name some.[1]

Besides acquiring the vector filed information, safety aspects of the equipment (e.g., due to high pulsed lasers), and availability of costly systems, the reliability and comparability of the measured vector fields with the simulation results are major issues since the assumptions made in the model often do not hold in reality. We address this issue by comparing two- and three-dimensional computational fluid dynamics (CFD) simulations with measured flow velocity field data and by establishing conditions for comparability.

To obtain the plane velocity field, we use the generally accepted PIV method.[2] For this purpose, small and light seeding particles, the so-called tracers, are usually injected into the flow to be investigated, which follow the flow. The tracers are illuminated by using a powerful light source (laser or LED), and their position is recorded by using a camera system that takes pairs of images in a very short time sequence.[3] Even though the theory of obtaining the velocity by analyzing the tracers' position is simple, the image acquisition of good quality makes professional systems costly. Since often high-speed cameras

synchronized with pulsed lasers are used, professional PIV systems easily start around 80 000 €, which makes it unaffordable for small research institutions or educational laboratories and is the main motivation of self-developed PIV systems.[4–6]

Our purpose is to set up a low-cost PIV system that is comparable to professional systems in terms of time resolution of the images and that can be safely used for educational purposes because no high-energy pulsed laser is required. The low-cost PIV system is tested on a laminar Couette flow and on a more complex flow scenario with obstacles (Sec. II). Additionally, in order to analyze the comparability of measured and computed velocity fields, a two-dimensional and three-dimensional CFD simulation of the Couette flow and the flow around obstacles is built up (Sec. III). For three different velocities, but still laminar flow behavior, and three obstacles placed one behind the other with two different shapes and varying distances, the velocity field along the gap height is compared (Sec. IV). In the conclusion (Sec. V), the main results are summarized, and comments are made on the applicability of the presented low-cost PIV system, as well as on the comparability of measurements and simulations.

II. EXPERIMENTAL SETUP

In Sec. II A and II B, the experimental setup, the components of the low-cost PIV system, and image processing are explained. The focus is on the individual parts of the measurement system and only on the most important information about the theoretical methods for image processing, as we have used a standardized procedure.

A. Test facility

A test rig is designed and built to generate an ideal Couette flow for which an exact solution of the Navier–Stokes equation exists so that the low-cost PIV system and our implemented CFD simulation can be validated against it. Obstacles can easily be added to the test rig to realize more complex flow scenarios.

In a fluid tank of glass with dimensions $300 \times 600 \times 300\,\mathrm{mm}^3$ (width × length × height), a frame made of aluminum profiles is inserted, to which the pulleys of a revolving conveyor belt are fixed; see Fig. 1. The conveyor is placed centrally in the tank and has a length of 500 mm and a width of 160 mm. The channel height between the conveyor belt and the bottom of the fluid tank is changeable in height and set to $H = 10\,\mathrm{mm}$ during the experiments. The rotational speed of the belt is adjustable between $n_{min} = 1\,\mathrm{min}^{-1}$ and $n_{max} = 180\,\mathrm{min}^{-1}$ by using a speed-controlled electric motor with a frequency converter, which with the selected transmission ratio of the toothed belt corresponds to a maximum belt speed of $U_{max} = 9.89 \times 10^{-1}\,\mathrm{ms}^{-1}$. The conveyor belt is completely immersed in the liquid inside the fluid tank and generates a constant flow velocity.

To ensure that laminar Couette flow is present even at large channel heights and high conveyor belt speeds, we used a higher viscosity glycerol–water mixture throughout the experiments. Table I shows the material data of the glycerol–water mixture at a room temperature of 20 °C (which is constant during all tests) derived from the correlations of Volk[7] and Cheng.[8] With the maximum belt velocity $U_{max} = 9.89 \times 10^{-1}\,\mathrm{ms}^{-1}$, channel height $H = 10 \times 10^{-3}\,\mathrm{m}$, and kinematic viscosity $\nu = 110 \times 10^{-6}\,\mathrm{m}^2\mathrm{s}^{-1}$, a maximum Reynolds number of $Re_{Exp,Max} = 89.96 < Re_{crit} = 300$ is present in the experiment, which is well below the problem-dependent critical Reynolds number $Re_{crit} = 300$ for a laminar Couette flow.[9]

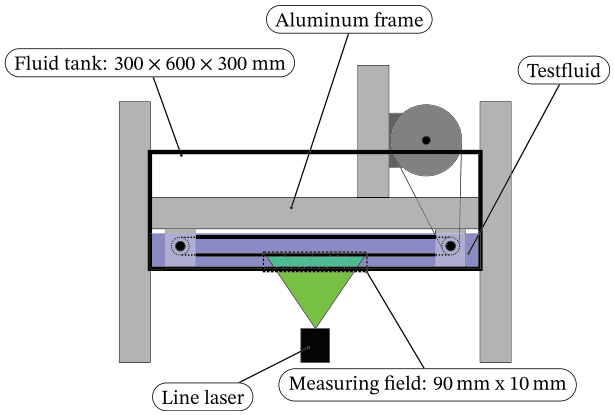

FIG. 1. Schematic representation of the test facility.

TABLE I. Physical properties of the glycerin–water mixture (86.5%) from the works of Volk[7] and Cheng[8] at the test condition.

Temperature T in °C	20
Density ρ in kg m^{-3}	1225
Dynamical viscosity η in Pa s^{-1}	1.35×10^{-1}
Kinematic viscosity ν in m^{2}s^{-1}	1.10×10^{-4}

In the first investigation, the velocity field of the Couette flow with the highest belt speed $U_{max} = 9.89 \times 10^{-1}\,\mathrm{ms}^{-1}$ is measured. After verifying that a Couette flow has been achieved, three square bars or hexagonal bars are placed at the bottom over the whole width of the fluid tank and aligned so that the obstacles are flowed over transversely, as illustrated in Fig. 2.

The height of the square bar is $H_\square = 6\,\mathrm{mm}$, and the vertical height of the hexagonal bar is $H_\bigcirc = 7\,\mathrm{mm}$. The three bars are aligned parallel to each other with a spacing as large as one square bar $\Delta x_{O,1} = H_\square$, a spacing twice as large as one square bar $\Delta x_{O,2} = 2 \cdot H_\square$, and a spacing three times as large as one square bar $\Delta x_{O,3} = 3 \cdot H_\square$ to observe the influence of the distances on the vortices in the spacing and their measurability with the low-cost PIV system. In addition, tests are carried out to determine whether different velocities have an

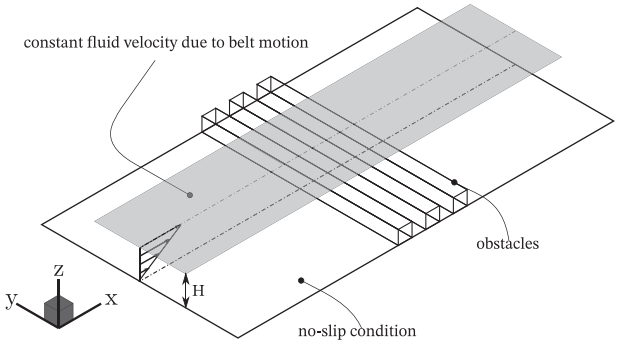

FIG. 2. Parallel aligned obstacles of the complex flow scenario.

influence on the quality of the measured flow profile, which should not actually be the case in the laminar range. Therefore, experiments are performed with three different belt speeds $U_1 = 55 \times 10^{-3}\,\mathrm{m\,s^{-1}}$ ($n_1 = 10\,\mathrm{min^{-1}}$), $U_2 = 110 \times 10^{-3}\,\mathrm{m\,s^{-1}}$ ($n_2 = 20\,\mathrm{min^{-1}}$), and $U_3 = 165 \times 10^{-3}\,\mathrm{m\,s^{-1}}$ ($n_3 = 30\,\mathrm{min^{-1}}$). To ensure steady-state flow conditions, in all cases, the velocity profile is recorded after at least 2 min running-in time for 10 s using the low-cost PIV setup. With respect to overflow over obstacles, the velocity $u(z)$ is analyzed as a function of channel height z at the center of the first distance at point A in Fig. 3 [see also Fig. 6(d)].

B. PIV setup

To measure two-dimensional velocity fields, the fluid under investigation is injected with tracer particles that follow the flow and are recorded by using a PIV system. Commercial PIV systems often combine a high-energy light source (often a neodymium YAG laser) with a high-speed camera.[3] The extremely high light energy required for high-speed imaging can be achieved by pulsing the laser. However, this requires precise synchronization with the camera and limits (along with the camera) the maximum detectable flow velocity. In addition, strict safety precautions must be taken for the use of high-energy pulsed lasers.

Since commercial closed-loop PIV systems are very expensive, we built a low-cost version consisting of the Chronos 1.4 high-speed camera (from Kron Technologies;[10] see Table III in the Appendix) and a 80 mW continuous class 2 diode line laser with a wavelength of 520 nm (IL-80-520 from MediaLas;[11] see Table IV in the Appendix). The built-in collimator creates a line of light without an additional system, so the laser continuously illuminates a plane in the center of the conveyor belt when placed under the glass fluid tank. The high-speed camera with a 35 mm Canon lens is positioned perpendicular to the flow on a guide rail at a distance of about 500 mm and records the fluid flow with a width of 90 mm. Figure 4 shows the final test setup. By focusing on the illuminated plane, the tracer's motion can be recorded in that plane and slightly ahead or behind it.

Most high-speed cameras suitable for PIV are based on a CCD or CMOS sensor. CCD sensors offer higher resolution compared to CMOS sensors, while CMOS sensors achieve higher frame rates.[3] The Chronos 1.4 high-speed camera is based on a CMOS sensor and offers frame rates up to 38 000 fps, making it well suited to capture extremely fast flow processes. The low acquisition cost also makes this camera ideal for upgrading existing systems to 3D stereo PIV. Table III in the Appendix shows some specifications of the camera. For the PIV

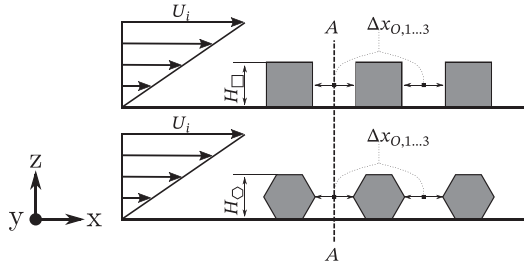

FIG. 3. Distance variation $\Delta x_{O,1}$ to $\Delta x_{O,3}$ of the obstacles. The dotted line $A - A$ shows the evaluation point for flow profiles.

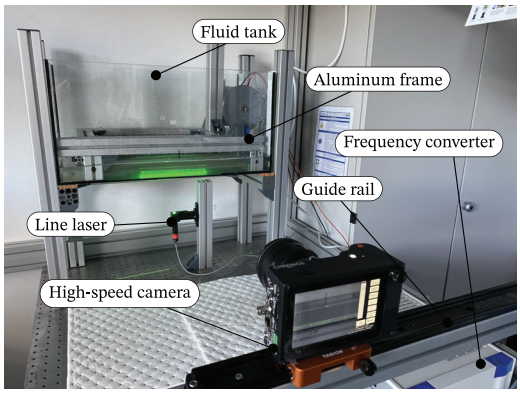

FIG. 4. Test facility for a Couette flow including the PIV system with a high-speed camera and line laser.

measurements, we used frame rates of 1057 fps in a resolution of 1280 × 1024 $\mathrm{px^2}$ of the image.

For the tracer (seeding particles), polyamide particles with a diameter of 100 μm (from LaVision[12]) are used. ∼5 g of the particles are injected into 5 L of the glycerol–water mixture and evenly distributed by stirring before the experiments. In order to not get any disturbing cross flow from the stirring, the conveyor belt is, then, started at the speed to be tested and allowed to run for 5 min before images are taken.

Summing up the costs of all relevant parts of the low-cost PIV system, which are independent of the test bench or the software for post-processing of the acquired images (see Table II), the total amount is about 4500 €, which is a fraction of commercial PIV systems. Compared to the already used low-cost PIV system,[4] the acquisition costs of our setup are twice as high, but we are not limited to low frame rates of 60 fps.

In a further step, the acquired images are post-processed to detect the position of tracers from two consecutive images, and the velocity of the tracers is calculated from the distance and time between the two images. There are a variety of commercial[13–15] and open-source[16,17] programs that strongly support automated post-processing.

For image processing, we use PIVlab, a freely available and open-source extension toolbox for MATLAB from Thielicke.[18] The toolbox is characterized by good usability and high functionality. In addition to various methods for determining the flow field, functions for image enhancement and error analysis are also available. Since the toolbox is completely based on MATLAB, own adaptations can also be implemented easily.

TABLE II. Price overview of used PIV components.

Camera	3360 €
Objective	530 €
Laser	450 €
Seeding particles	100 €
Total	4440 €

The most relevant part of the PIV analysis is the cross correlation of two images to detect the tracer motion.[3] This involves searching for a repeating pattern within a query window of image $A(m, n)$ and image $B(m, n)$. Specifically, the solution is the discrete cross correlation function,[3]

$$R_{II}(x,y) = \sum_{i=-K}^{K}\sum_{j=-L}^{L} I(i,j)I'(i+x,j+y), \tag{1}$$

which computes the cross correlation matrix $R_{II}(x, y)$ from the intensity values $I(i, j)$ and $I'(i + x, j + y)$ of the image pairs. The maximum value of the matrix $R_{II}(x, y)$ indicates the most likely shift of the tracer from image A to B. To determine the correlation matrix, PIVLab offers single-pass direct cross correlation (DCC) and multiple-pass direct Fourier transform correlation with window fitting (FFT window deformation). Since version 2.30, an ensemble correlation is also available. These methods differ in accuracy and computational effort.

Due to its wide applicability and generally good results, we have used the FFT-based cross correlation for image processing. Therefore, the cropped image is decomposed into several sections (query area) to which the cross correlation is applied, and one velocity vector is determined for each section. Since cross correlation is more robust for larger query areas, they are set to 30 × 30 px^2 in the first pass, as exemplified in Fig. 5, although only limited velocity information is obtained. In a second pass, the size of the query regions is reduced to 20 × 20 px^2 to obtain a more detailed velocity field. The PIVlab post-processing settings we use are from previous test runs but can be changed individually. Besides the customized query area, we used the default values of the toolbox with good results. For more detailed mathematical background information on the methods and advanced settings for image processing, refer to the work of Raffel[3] and the contribution of Thielicke[18] as well as to the manual of the selected software since a detailed description is beyond the scope of this paper.

Finally, the results of the velocity field must be checked for plausibility. Outliers can be caused by a faulty cross correlation that incorrectly assigns the tracers. To exclude these outliers, in addition to the threshold filter and media test, custom velocity bounds can be defined

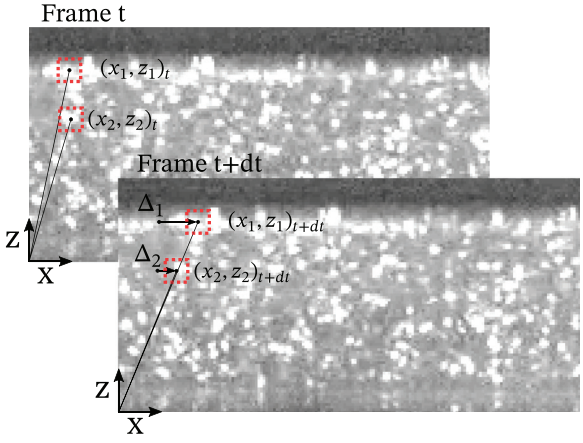

FIG. 5. Representative image of the experiment: Evaluate displacements Δ_i of tracers through the FFT.

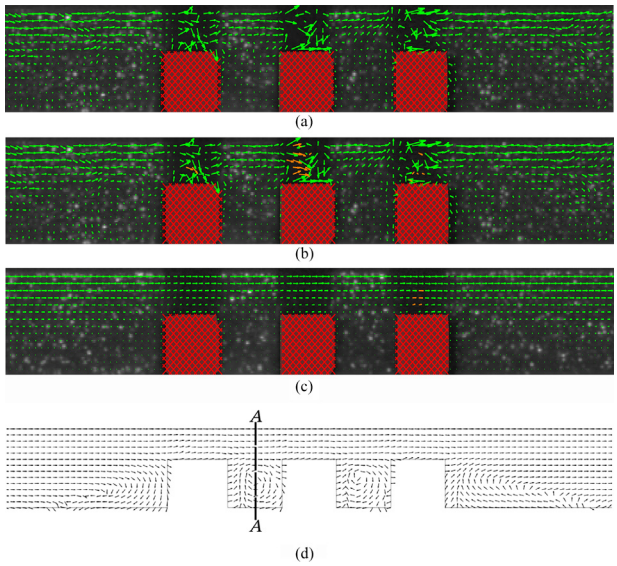

FIG. 6. PIV processing workflow from raw image data to the vector field with following substeps: (a) Vector field after cross correlation. (b) Vector field after the validation step (filtering and interpolation of missing vectors). (c) Averaged vector field from all image pairs. (d) Further processing of the data in Paraview and evaluation point $A - A$ for further investigations.

from a scatterplot in PIVlab. In our case, the velocity field was filtered with a lower u_{min} and upper u_{max} threshold of velocity,

$$u_{min} = \overline{u} - m \cdot \sigma_u, \tag{2}$$

$$u_{max} = \overline{u} + m \cdot \sigma_u. \tag{3}$$

Here, $\overline{u}$ represents the mean flow velocity, σ_u represents the standard deviation of u, and m represents the filter strength. For the analysis of the experimental data, we used the default value of $m = 7$. In the last step, missing velocity vectors are linearly interpolated, and the mean velocity for each point in the vector field is determined from all evaluated images. This completes the PIV workflow (Fig. 6), and the results can be exported to a visualization application, such as ParaView,[19] for further processing.

III. NUMERICAL SETUP

To explore quantitative results and possible limits of our low-cost PIV setup, a computational fluid dynamics (CFD) simulation was performed. For this purpose, the C++ toolbox OpenFOAM[20] (V1906) is used, which solves the Navier–Stokes and the continuity equation using the finite volume method. Since Couette flow describes the planar, steady-state flow of a fluid between two parallel plates with infinite extension (no cross flow effects), we first built two-dimensional analog models of the experiments in OpenFOAM. In order to represent the experimental test facility more realistically, additional three-dimensional models are developed. In both cases, the length and height of the investigated fluid area correspond to the conveyor belt length and channel height with 500 × 10 mm^2. For the three-dimensional model, the width of the fluid reservoir with 160 mm has been additionally considered, in which a constant velocity is applied in

an area equivalent to the reduced width of the conveyor belt over 150 mm (to save elements and thus calculation time).

In order to ensure a sufficient resolution of the flow field and to achieve a mesh-independent solution, a mesh study was carried out in advance. In general, the surface and mesh generation are fully automated and parameter controlled. The channel geometry and the number of nodes along the channel height have been given as input parameters. Then, the global element size for a coarse mesh (equidistant mesh) and corresponding node numbers for channel depth and channel length have been calculated. In areas where high flow deflections are expected (around obstacles), the mesh is refined by a factor of 2 in the number of nodes. As a result of the mesh study, the element size is shown to be 333×10^{-3} mm (30 elements along the height $H = 10$ mm of the channel) for the finer mesh and 666×10^{-3} mm for the slightly coarser mesh in the peripheral areas. Figure 7 shows the final hex-dominant mesh of the three-dimensional model.

It is assumed that the flow is stationary and laminar. This applies to moderate belt velocities and after a sufficient run-in time at the beginning of the experiments. To exclude inflow and outflow effects, periodic inflow and outflow boundaries are defined in addition to a large channel length. A no-slip condition is defined at the bottom of the glass fluid tank, at the obstacle surfaces, and at the lateral area boundaries (walls of fluid tank). Assuming no slip between the conveyor belt and fluid, the belt velocity is modeled as a constant fluid velocity in the positive x direction at height H of the channel. The pressure boundary conditions are set according to the velocity boundary conditions. A second order upwind method is used for the advective terms of the Navier–Stokes equations, and the *smoothSolver* with the *GaussSeidel* smoother is used to solve the system of equations. The required pressure–velocity coupling is realized by the *SIMPLE* approach. However, due to the assumption of laminar flow, turbulent terms are neglected.

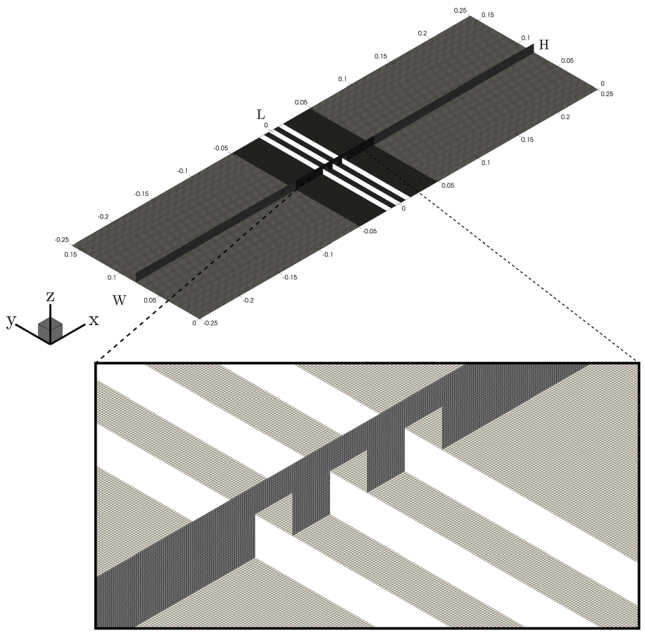

FIG. 7. Used mesh of the CFD simulation.

IV. RESULTS

After the experiments were conducted and the flow field was measured as well as calculated by the CFD simulation, the results are compared for different scenarios. First, a laminar Couette flow is used to determine the degree of idealization of the 2D CFD simulation and the recording quality of the experiment's PIV system, before a flow over obstacles with different settings is investigated and compared with the additionally developed 3D CFD model.

A. Validation: Laminar Couette flow

The Couette flow is one of the rare analytical solutions of the Navier–Stokes equation.[21] It is formed between two oppositely moving, flat plates. For plats with infinite width and distance H in the positive z-direction and neglecting pressure gradients or external forces, the Navier–Stokes equation is simplified to an ordinary differential equation of second order for the steady-state laminar case. The boundary conditions of the velocity with $u(0) = 0$ and $u(H) = U$ can be formulated with the no-slip condition at the ground and the belt speed U,

$$\frac{d^2u}{dz^2} = 0, \text{ with } u(0) = 0, \; u(H) = U. \tag{4}$$

Thus, integrating Eq. (5) two times, the exact solution of $u(z)$[21]

$$u(z) = U \cdot \frac{z}{H} \tag{5}$$

is obtained. The solution $u(z)$ yields a flow velocity, which increases linearly above the channel height. The maximum Reynolds number $Re_{Exp,Max} = 89.96$ in the experiment is far below the critical Reynolds number $Re_{crit} = 300$ for a laminar Couette flow, so the analytical solution can be used to validate the PIV analysis.

Figure 8 shows the velocity profile along the height of the channel of the analyzed images acquired with the low-cost PIV system and the analytical solution, which is a linear function from the zero velocity at the bottom of the fluid tank to $u(H) = U_{max}$ of the conveyor belt at top.

The experimental results show a very good correlation with the analytical Couette flow, which, on the one hand, ensures that the designed test facility is suitable to realize laminar flow in a channel

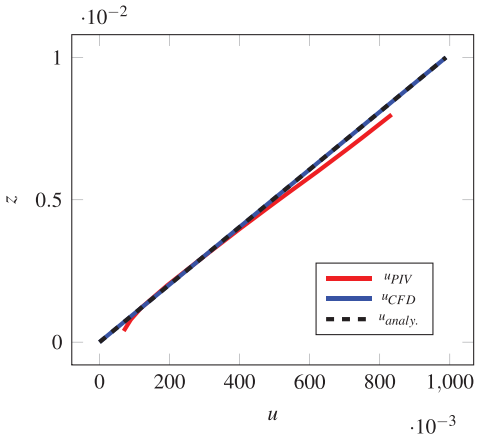

FIG. 8. Laminar Couette flow at $Re_{Exp,Max} = 89.96$: measured flow (u_{PIV}) vs CFD solution (u_{CFD}) vs analytical solution (u_{analy}).

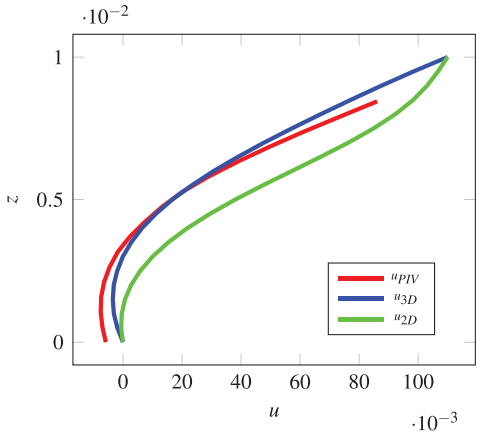

FIG. 9. Velocity profile comparison: 2D-vs 3D-CFD simulations vs PIV measurement in the first cavity (position *A*) for the overflows of the square bars with $\Delta x_{O,2}$ and U_2.

and, on the other hand, that the presented low-cost PIV system can capture the velocity field sufficiently well. In Fig. 8, it is noticeable that the velocity profile by the PIV measurement does not cover the entire channel height, which is due to the image processing. Since only one velocity value is determined for each interrogation area (20×20 px^2), this value is placed in the center of the area, resulting in missing values at the transition areas between fluid and surfaces. The larger area of velocity values missing at the transition to the conveyor belt is additionally due to reflections of the laser light so that here the motion of the tracers could only be evaluated to a limited extent.

B. Laminar flow over square and hexagonal obstacles

After validating the PIV system with the Couette flow, the next step is to successfully measure overflows over obstacles, which are common in engineering. Examples include overflowing a building[22,23] or over a highly idealized rough surface.[24] Following this, the setup is now modified by three square ($H_{\square} = 6$ mm) and, for more complex applications, hexagonal bars ($H_{\hexagon} = 7$ mm), creating two cavities each. By flowing around the obstacles, in addition to separation and vortices, the influence of the second cavity on the first one can be studied. For this purpose, the distance between the obstacles is varied between 6 mm and 18 mm in three steps. To assess the acquisition quality at higher flow velocities, which should not change the overall flow

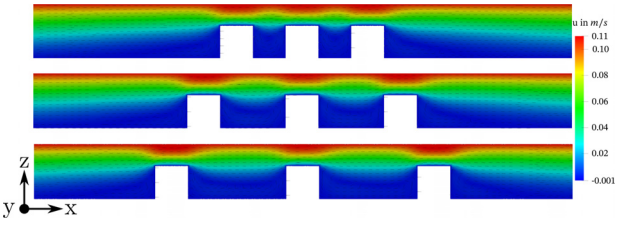

FIG. 10. CFD velocity fields at $U_2 = 110 \times 10^{-3}\,\mathrm{m\,s^{-1}}$ and $\Delta x_{O,1}$, $\Delta x_{O,2}$, and $\Delta x_{O,3}$.

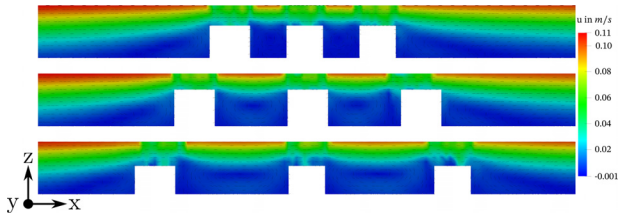

FIG. 11. PIV velocity fields at $U_2 = 110 \times 10^{-3}\,\mathrm{m\,s^{-1}}$ and $\Delta x_{O,1}$, $\Delta x_{O,2}$, and $\Delta x_{O,3}$.

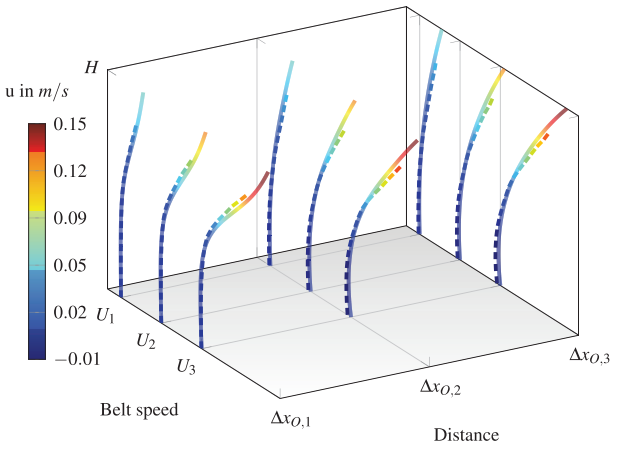

FIG. 12. Comparison of PIV measurement (dashed line) and CFD result (solid line) of the velocity profile from the center of the first cavity (position *A*) for the overflows of the square bars.

behavior in the laminar case, the images are taken at three different belt velocities $U_1 = 55 \times 10^{-3}\,\mathrm{m\,s^{-1}}$ ($n_1 = 10\,\mathrm{min^{-1}}$), $U_2 = 110 \times 10^{-3}\,\mathrm{m\,s^{-1}}$ ($n_2 = 20\,\mathrm{min^{-1}}$), and $U_3 = 165 \times 10^{-3}\,\mathrm{m\,s^{-1}}$ ($n_3 = 30\,\mathrm{min^{-1}}$). The corresponding velocity profiles along the height of

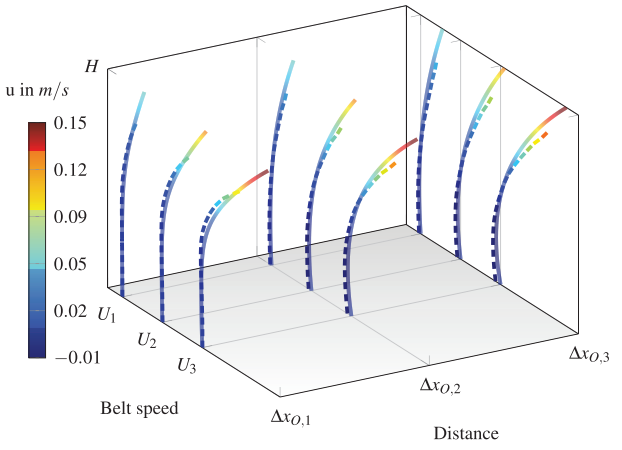

FIG. 13. Comparison of PIV measurement (dashed line) and CFD result (solid line) of the velocity profile from the center of the first cavity (position *A*) for the overflows of the hexagonal bars.

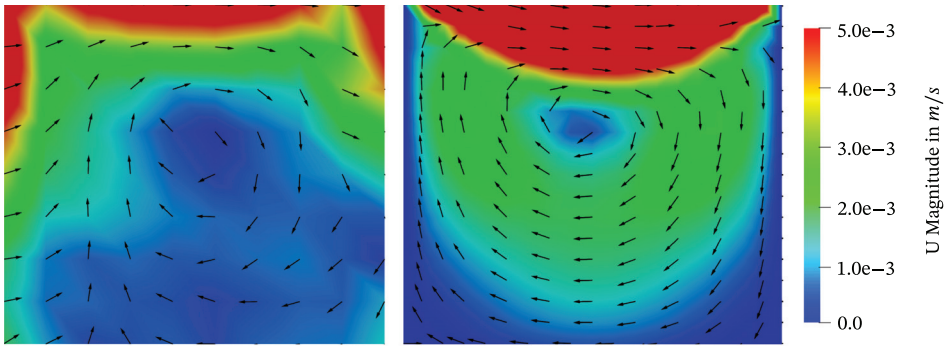

FIG. 14. Comparison of the vortex structures of experiment (left) and simulation (right) for the overflow of square bars with a belt speed of $U_1 = 55 \times 10^{-3}\,\mathrm{m\,s^{-1}}$ and distance $\Delta x_{O,1} = H_{\square}$.

the channel are compared at the center of the first cavity, at position A [see Figs. 3 and 6(d)].

Figure 9 shows velocity profile plots at position A of the belt velocity $U_2 = 110 \times 10^{-3}\,\mathrm{m\,s^{-1}}$ from the recorded position of the traces during the experiments and from the two- and three-dimensional CFD simulations. Comparing the velocity profiles, a large discrepancy between the two-dimensional model and the other results is obvious. Since the three-dimensional model and the experimentally obtained velocity field show good agreement, the errors must result from the assumptions of the 2D model. One assumption is the infinite width of the conveyor belt, which excludes cross flows, but which can occur in reality. Considering these cross flows, agreement of the results from the three-dimensional model and the PIV experiment is remarkable.

The comparison of the velocity fields (Figs. 10 and 11) of measurement and three-dimensional CFD simulation for $U_2 = 110 \times 10^{-3}\,\mathrm{m\,s^{-1}}$ clearly shows that the overall flow characteristic and details can also be captured with the low-cost PIV system.

Vortices created between the obstacles can be visualized by the tracer motion on the captured images and allow a detailed analysis of the flow profile. The vortex structures, the velocity magnitudes, and the resting vortex eye are comparable between simulation and PIV measurements. Surrounding areas, however, have a larger deviation from the simulation. The inaccuracies at the rigid-body edges of the obstacles or the fluid tank are most probably caused by the very low flow velocities and the resulting small movements of the tracers. Inaccuracies in the transition area to the conveyor belt might also be induced by the small number of tracers to be evaluated. However, by adding smaller tracer particles (e.g., 10 μm) and increasing their quantity, the evaluation quality can be improved. In addition, the resolution of the velocity field can be enhanced by smaller evaluation windows for the cross correlation, which also reduces inaccuracies in the transition between fluid and the wall.

Finally, all nine velocity profiles from measurement and simulation are spatially plotted for square bars in Fig. 12 and for hexagonal bars in Fig. 13. The abscissas correspond to the selected speeds U_i, and the ordinates correspond to the distances $\Delta x_{O,i}$ of the obstacles to each other. Thus, the influence of speed and distance on the flow profile can be determined directly. In general, all profiles show a high degree of agreement between experiment and simulation. For small distances between obstacles, a very flat flow profile can be recognized, which becomes more and more convex as the distance between the obstacles increases. The maximum flow velocity is always reached at the highest point of the channel and corresponds to the adjusted belt speed. In the lower area, a negative velocity is observed and indicates a vortex, which changes according to the distance of obstacles, as illustrated exemplary for $U_1 = 55 \times 10^{-3}\,\mathrm{m\,s^{-1}}$ and $\Delta x_{O,1} = H_{\square}$ in Fig. 14. Even though the general flow behavior does not change at different belt speeds in the laminar case, the influence of obstacle spacing on vortex formation (especially in the second interstitial space) is clearly visible in the CFD simulation and measurable by using the presented PIV system.

V. CONCLUSION

In this work, a low-cost PIV system for the measurement of laminar flow fields was presented and tested against simulations. As a first validation, a laminar Couette flow was considered for which an experimental setup was developed. In this first test, the flow profile of the experiment and the analytical solution agrees very well. To test the application for more complex flows, a second experiment was conducted to study a flow over an array of obstacles. Well-resolved steady-state two- and three-dimensional CFD simulations serve as benchmarks. High agreement between experiment and 3D CFD simulation is also observed in the second case. Less good agreement was only found at the edges to rigid walls and in the vortex region. The main reasons for this are supposed to be the limited number of tracers that can be evaluated, the small position difference between the tracers, and the size of the interrogation area during image processing. Despite the mentioned weaknesses at the edges, the overall characteristic can be measured very reliably with the presented low-cost PIV system.

The comparison with CFD simulations shows that the presented PIV system, consisting of a continuous line laser and a high-speed camera with a commercially available photo lens for a total of 4440 €, provides very good evaluable images and, thus, represents a good alternative to very expensive commercial systems. In addition, due to the moderate power unpulsed laser, no synchronization or special safety precautions need to be considered for the operation of the PIV system, which makes it attractive for small research facilities or teaching institutes.

However, the comparison between measured velocity fields and two-dimensional CFD simulations with obstacles also clearly shows that even for simple flow scenarios, the simulation quickly misrepresents the measured reality if oversimplifications or incorrect assumptions are made. A comparison of the simulation results with reality is, therefore, always advisable and feasible with the presented PIV system.

Due to the very fast exposure time of the high-speed camera used, it should also be possible to successfully detect turbulent flows, and because of the low acquisition costs, even a simple conversion to 3D PIV should be possible.

ACKNOWLEDGMENTS

This study was funded by the Deutsche Forschungsgemeinschaft (DFG, German Research Foundation)—Project No. 172116086—SFB 926.

APPENDIX: INFORMATION OF THE USED COMPONENTS IN PIV SETUP

In order to be able to replicate the low-cost PIV system, we provide here the most important information about the components used.

1. High-speed camera Chronos 1.4 (Table III and Fig. 15)

TABLE III. Camera specification of Chronos 1.4.[10]

Resolution (max)	1280 × 1024 px^2 at 1057 fps
Resolution (min)	336 × 96 px at 38 868 fps
Speed	1.4 Gpx/s
ISO	Mono - ISO 740–11 840
Shutter	Electronic global shutter, 1/fps to 1 μs
Dynamic range	56.7 dB
Bit depth	12-bit

FIG. 15. Chronos 1.4 high-speed camera from Kron Technologies in front view.

2. Continuous line laser IL-80-520 (Table IV and Fig. 16)

TABLE IV. Specification of continuous line laser IL-80-520.[11]

Laser power:	∼80 mW
Wavelength:	520 nm GREEN
Deflection angle:	60°
Laser class:	1/2, depending on installation
Trigger input:	Optional, 4 V–25 V = on, 0 V = off
Lifetime:	typ. > 25 000 h
Temperature range:	∼15 °C to +40 °C

FIG. 16. Line laser of the company MediaLas with a wavelength of 520 nm and a power of 80 mW, article number: IL-80-520.[11]

DATA AVAILABILITY

The data that support the findings of this study are available from the corresponding author upon reasonable request.

REFERENCES

[1]J. P. Holman, *Experimental Methods for Engineers* (McGraw-Hill, 2001).
[2]R. J. Adrian, "Particle-imaging techniques for experimental fluid mechanics," Annu. Rev. Fluid Mech. **23**, 261–304 (1991).
[3]M. Raffel, C. E. Willert, F. Scarano, C. J. Kähler, S. T. Wereley, and J. Kompenhans, *Particle Image Velocimetry* (Springer International Publishing, 2018).
[4]A. Budd and J. Howison, "A low-cost PIV system for undergraduate fluids laboratories," in *Proceedings of American Society for Engineering Education Annual Conference and Exposition* (American Society for Engineering Education, Salt Lake City, UT, 2018).
[5]*Design and Implementation of a Low-Cost Particle Image Velocimetry System for Undergraduate Research and Education*, edited by B. Ring and E. Lemley (ASEE Conferences, 2014).
[6]W. G. Ryerson and K. Schwenk, "A simple, inexpensive system for digital particle image velocimetry (dpiv) in biomechanics," J. Exp. Zool., Part A **317**, 127–140 (2012).
[7]A. Volk and C. J. Kähler, "Density model for aqueous glycerol solutions," Exp. Fluids **59**, 75 (2018).
[8]N.-S. Cheng, "Formula for the viscosity of a glycerol-water mixture," Ind. Eng. Chem. Res. **47**, 3285–3288 (2008).
[9]M. Couliou and R. Monchaux, "Large-scale flows in transitional plane Couette flow: A key ingredient of the spot growth mechanism," Phys. Fluids **27**, 034101 (2015).
[10]Kron Technologies Inc., Chronos 1.4 datasheet - Kron Technologies, 2020.
[11]M. L. Electronics GmbH, Technische Information Zum Linienlaser Artikelnummer:IL-80-520 - MediaLas, 2019.
[12]LaVision GmbH, Seeding particles - LaVision, 2020.

[13]Dantec Dynamics A/S, DynamicStudio - Dantec Dynamics, 2020.
[14]ILA_5150 GmbH, PIV Post-processing Software PIVview - ILA_5150, 2020.
[15]LaVision GmbH, DaVis Software Solution for Intelligent Imaging - LaVision, 2020.
[16]J. K. Sveen, "An Introduction to MatPIV V. 1.6.1," Preprint Series. Mechanics and Applied Mathematics, http://urn.nb.no/URN:NBN:no-23418, 2004.
[17]Z. J. Taylor, R. Gurka, G. A. Kopp, and A. Liberzon, "Long-duration time-resolved PIV to study unsteady aerodynamics," IEEE Trans. Instrum. Meas. **59**, 3262–3269 (2010).
[18]W. Thielicke and E. J. Stamhuis, "PIVlab towards user-friendly, affordable and accurate digital particle image velocimetry in MATLAB," J. Open Res. Software **2**, e30 (2014).
[19]J. Ahrens, B. Geveci, and C. Law, "ParaView: An end-user tool for large-data visualization," in *Visualization Handbook* (Elsevier, 2005), pp. 717–731.
[20]H. G. Weller, G. Tabor, H. Jasak, and C. Fureby, "A tensorial approach to computational continuum mechanics using object-oriented techniques," Comput. Phys. **12**, 620 (1998).
[21]H. Schlichting and K. Gersten, *Grenzschicht-Theorie*, 10th ed. (Springer, 2006).
[22]R. Gnatowska, M. Sosnowski, and V. Uruba, "CFD modelling and PIV experimental validation of flow fields in urban environments," in E3S Web of Conferences (EDP Sciences, 2017), Vol. 14, p. 01034.
[23]M. K.-A. Neophytou, C. N. Markides, and P. A. Fokaides, "An experimental study of the flow through and over two dimensional rectangular roughness elements," Phys. Fluids **26**, 086603 (2014).
[24]J. Ou and J. P. Rothstein, "Direct velocity measurements of the flow past drag-reducing ultrahydrophobic surfaces," Phys. Fluids **17**, 103606 (2005).